JAMES | Journal of Advances in Modeling Earth Systems

RESEARCH ARTICLE
10.1029/2020MS002260

A Stochastic Parameterization of Organized Tropical Convection Using Cellular Automata for Global Forecasts in NOAA's Unified Forecast System

Lisa Bengtsson[1,2], **Juliana Dias**[2], **Stefan Tulich**[1,2], **Maria Gehne**[1,2], **and Jian-Wen Bao**[2]

[1]CIRES, University of Colorado, Boulder, CO, USA, [2]NOAA ESRL PSL, Boulder, CO, USA

Key Point:

- A cellular automaton was successfully introduced to the NOAA Global Forecast System's operational deep cumulus convection scheme
- Enhanced sub-grid organization provided by the cellular automaton lead to improved spatial and temporal correlation scales of modeled precipitation
- Self-organizing cellular automata for representation of convective organization is beneficial for the model's ability to reproduce the observed large-scale organization of convectively coupled waves

Correspondence to:
L. Bengtsson,
lisa.bengtsson@noaa.gov

Citation:
Bengtsson, L., Dias, J., Tulich, S., Gehne, M., & Bao, J.-W. (2021). A stochastic parameterization of organized tropical convection using cellular automata for global forecasts in NOAA's Unified Forecast System. *Journal of Advances in Modeling Earth Systems*, *13*, e2020MS002260. https://doi.org/10.1029/2020MS002260

Received 24 JUL 2020
Accepted 3 DEC 2020

Abstract In the atmosphere, convection can organize from smaller scale updrafts into more coherent structures on various scales. In bulk-plume cumulus convection parameterizations, this type of organization has to be represented in terms of how the resolved flow would "feel" convection if more coherent structures were present on the subgrid. This type of subgrid organization acts as building blocks for larger scale tropical convective organization known to modulate local and remote weather. In this work a parameterization for subgrid (and cross-grid) organization in a bulk-plume convection scheme is proposed using the stochastic, self-organizing, properties of cellular automata (CA). We investigate the effects of using a CA which can interact with three different components of the bulk-plume scheme that modulate convective activity: entrainment, triggering, and closure. The impacts of the revised schemes are studied in terms of the model's ability to organize convectively coupled equatorial waves (CCEWs). The differing impacts of adopting the stochastic CA scheme, as compared to the widely used Stochastically Perturbed Physics Tendency (SPPT) scheme, are also assessed. Results show that with the CA scheme, precipitation is more spatially and temporally organized, and there is a systematic shift in equatorial wave phase speed not seen with SPPT. Previous studies have noted a linear relationship between Gross Moist Stability (GMS) and Kelvin wave phase speed. Analysis of GMS in this study shows an increase in Kelvin wave phase speed and an increase in GMS with the CA scheme, which is tied to a shift from large-scale precipitation to convective precipitation.

Plain Language Summary Vertical heat transfer between the ocean and atmosphere, called atmospheric convection, can organize over a variety of different scales, ranging from small-scale fair-weather cumulus clouds, rain showers and thunderstorms, to large scale "convectively coupled" equatorial waves. In traditional weather and climate models, such organization is not well represented, as only the mean effect of all possible convective types occurring in a model grid-box is represented by a one-dimensional plume model. In this study we explore the impact of representing convective organization in weather and climate models using cellular automata—a discrete model often used to describe self-organizing behavior in physical systems. We are particularly interested in the impact of the proposed method in the tropics since the weather in the tropics is dominated by organized atmospheric convection, and serves as the engine of the Earth's atmospheric circulation pattern. We find that when we let the cellular automata initiate atmospheric convection in the nearby environment of existing precipitating convection, precipitation becomes more organized in space and time, and there is an improvement in the model's ability to reproduce the observed large-scale organization of convectively coupled tropical variability, important for improving predictions of weather and climate across the world.

1. Introduction

Atmospheric convection is generally organized over a variety of different time and space scales, ranging from small-scale cold pool driven organization to mesoscale convective systems to synoptic and planetary waves. Several physical processes have been shown to organize convection from random clouds into more coherent structures, including ambient vertical wind-shear together with convectively generated density currents and gravity waves (e.g., Houze et al., 2004; Huang, 1984; Moncrieff et al., 2012; Schiro & Neelin, 2019; Tompkins, 2001). In the tropics, coherent wavelike disturbances coupled to atmospheric convection on the synoptic scale can often be tracked for days or even weeks, referred to as "convectively coupled equatorial waves" (CCEWs). Modeling the onset and propagation of CCEWs has historically posed

substantial challenges in the numerical weather prediction community (e.g., Kiladis et al., 2009; Wheeler & Kiladis, 1999; Zhang et al., 2005) and predictions made using NOAA's Unified Forecast System (UFS) are no exception (e.g., Bengtsson, Dias, et al., 2019; Dias et al., 2018). Accurate representation of CCEWs in global numerical weather and climate models is important because it has been shown that improved modeling of tropical weather can ultimately lead to better predictions of weather in the extratropics, via Rossby wave teleconnections (e.g., Jones et al., 2011; Jung et al., 2010, 2011; Schreck et al., 2013).

Despite intense effort aimed at elucidating the mechanisms of convective organization, the practical problem of representing such organization in subgrid parameterizations in global models has received relatively little attention in the literature. A few examples of schemes proposed for parameterizing the effects of convective organization in global GCM's are those described in Donner (1993), Donner et al. (2001), Mapes and Neale (2011), Park (2014) and Moncrieff et al. (2017).

In Moncrieff et al. (2017) a method of parameterizing the physical and dynamical effects of convective organization on the environment was proposed, referred to as multiscale coherent structure parameterization. The proposed scheme adds the hypothesized missing process of slantwise overturning by adding top-heavy heating and upgradient momentum transport as effects of organized convection. The scheme is based on the argument that slantwise overturning is the mesoscale response of an ensemble of cumulonimbus in sheared environments.

Mapes and Neale (2011) proposed that the effect of convective organization can be captured in terms of convective area coverage, net vertical mass flux and entrainment/detrainment profiles of plumes. Their work is based on the notion that, in bulk-plume models, there is no difference in how individual smaller scale plumes are spatially arranged, as the full ensemble of convective updrafts is represented by a one-dimensional single mean updraft/downdraft model. They outlined an idea for convective subgrid organization that would alter the convective parameterization through: (1) enhanced plume overlap, (2) wider plumes with less lateral mixing, (3) the areal coverage—effectively the plume-base mass-flux, and (4) preferential growth of convection in preconditioned areas near prior plumes (trigger). More recently, this conceptual approach has been adopted in the Unified Convection Scheme (UNICON; Park, 2014), where subgrid mesoscale convective organization is parameterized through a specified dependence on subgrid mesoscale density currents. UNICON has demonstrated the importance of parameterized convective organization to improve GCMs in simulating tropical variability, without degrading the mean state, as a consequence of enabling convection schemes to represent a wide range of types of plumes that play different roles in the atmosphere (Ahn et al., 2019).

In a similar effort, but for regional numerical weather prediction (NWP) simulations with horizontal grid-spacings of less than 10 km, Bengtsson et al. (2013) proposed to enhance subgrid convective organization using a stochastic, self-organizing cellular automata (CA) simulated on the subgrid of the numerical weather model grid, providing a simple model for subgrid, and cross-grid, convective organization and stochasticity. In this scheme, the fractional area covered by subgrid CA cells was conditioned on Convective Available Potential Energy (CAPE) and specified as a source/sink term in the prognostic equation used to predict cloud-base convective area fraction in the convection parameterization "3MT" (Gerard et al., 2009). Since the study was carried out in a regional gray-zone resolution model over Europe, the scheme has not been evaluated in terms of precipitation organization in a global model where organized convection tends to strongly couple with the general circulation of the tropical atmosphere. The idealized study by Bengtsson et al. (2011), which investigated idealized (shallow-water model) simulations initialized with equatorial wave modes, provides evidence that the cellular automaton might be beneficial for simulations of tropical large-scale convective organization. In that study, the CA allowed for stronger interaction between the simulated subgrid scales and the large-scale flow, as opposed to a small-scale random forcing.

In light of the results found in the idealized framework, our goal here is to study the impact of the CA on organizing convective precipitation into larger coherent structures, and the impact of enhanced subgrid and cross-grid organization of parameterized cumulus convection on the simulation of CCEWs in an NWP framework. To achieve this goal, we extend the CA scheme presented in Bengtsson et al. (2013), motivated by the subgrid organization schemes presented by Mapes and Neale (2011) and Park (2014), and we evaluate the impact in a global forecast model with horizontal grid-spacing of ~25 km. We use the NOAA UFS,

which is an operational global model that employs a "conventional" cumulus parameterization, based on a bulk mass-flux entraining plume model (Han et al., 2011). We condition the CA on the UFS subgrid scale rain evaporation—as this is a criterion for subgrid density currents initiated by convective cold pools - and explore its impact on convective organization when allowed to interact with one of three different components of the cumulus convection scheme: (1) triggering, (2) closure, and (3) plume model (entrainment). Since the CA can organize across adjacent model grid-boxes, the triggering application represents an enhanced onset of convective updrafts if they are being triggered in spatial clusters. The closure application represents larger subgrid convective areal coverage, leading to stronger mass-flux at cloud-base. Lastly, the application with the plume-model represents the tendency of organized subgrid convection to have wider plumes, such that enhanced organization by the CA leads to less fractional entrainment. We evaluate the performance of the scheme, and the different coupling strategies by assessing the model's ability to organize and propagate CCEWs, and its impact on the Normalized Gross Moist Stability (NGMS), introduced later in this study, as well as on vertical heating profiles.

To complement this analysis, we also compare the sensitivity of modeled CCEWs when using the CA convection scheme, and the different methods of coupling to the convection scheme, to that of more standard stochastic physics. Specifically, it has been shown that stochastic physics included in global models by perturbing the physics tendencies that are produced by the physics parameterizations with a spatially and temporally correlated random pattern on the synoptic scales, referred to as the Stochastically Perturbed Physics Tendency (SPPT) scheme (Buizza et al., 1999; Lutbecher et al., 2017; Palmer et al., 2009) can improve tropical variability in seasonal and decadal predictions, including the Madden Julian Oscillation (MJO) (Kessler & Kleeman, 2000; Vitart & Molteni, 2010) and the El Nino Southern Oscillation (ENSO) (e.g., Christensen et al., 2016; C. Yang et al., 2019). Since the CA scheme addresses both enhanced organization of convection, and a stochastic method to represent the production and destruction of subgrid convective elements that can, in a limited sense, produce a plume distribution variability in the parameterization itself, this "process-level" approach can be seen as more physically motivated, compared to perturbing the tendency computed by the parameterization a-posteriori with a value between 0 and 2. Thus, we here investigate if the CA scheme can provide any additional value in terms of simulating CCEWs, compared to the more established SPPT methodology. It should be noted, however, that in terms of standard ensemble metrics such as the relationship between spread and skill between atmospheric model state variables, previous studies have shown that the CA alone does not produce enough upscale error growth to sufficiently provide robust uncertainty estimates from cumulus convection on the synoptic scales, as can be given by SPPT which perturbations are introduced on the synoptic scale (Bengtsson & Körnich, 2016; Bengtsson, Bao, et al., 2019; Bengtsson, Dias, et al., 2019). The focus here is the impact of the schemes on simulations of organization and propagation of CCEWs.

2. Methodology

2.1. A Cumulus Convection Subgrid Organization Scheme

The representation of multiple plumes and the interactions among them within an NWP model grid-box may be regarded as a form of cloud population dynamics (e.g., Neggers, 2015), and several stochastic birth/death models for cloud population have been explored within the NWP community. Such models are useful for simulating competing processes seen in nature, such as production versus dissipation of clouds (Hagos et al., 2018; Neggers, 2015; Plant, 2012). Other models considered for birth/death processes used for cloud population in a grid-box are Markov chains and CA. A Markov chain is a mathematical system that undergoes transitions from one discrete state to another, and the probabilities associated with the various state changes are called transition probabilities. An example of this approach is the parameterization describing the convective state of the entire model column as a discrete Markov chain (e.g., Dorrestijn et al., 2013, 2015; Gottwald et al., 2016; Khouider et al., 2010). Markov chains that considers the state of its neighborhood in their transition probability formulation are stochastic CA, which are often used as simple mathematical models to simulate spatial self-organizational behavior. A CA describes the evolution of discrete states on a lattice grid. The states are updated according to a set of rules based on the states of neighboring cells at the previous time step. In addition to memory, cellular automata can allow for lateral communications between neighboring grid boxes, and can thus introduce spatial self-organization. In convective parameterizations,

it has been found beneficial for enhancing the large-scale response from diabatic processes in an idealized shallow water framework by increasing the upscale cascade of kinetic energy from smaller to larger atmospheric scales when more organization is present. It can also enhance convective organization to form squall-lines in regional NWP simulation at gray-zone resolutions, and increase the ensemble spread associated with uncertainty in convective parameterizations (Bengtsson & Körnich, 2016; Bengtsson, Bao, et al., 2019; Bengtsson et al., 2011, 2013). In addition, Böing (2016) presents evidence that CA (which uses particles as well as grid cells in a hybrid method) can be used to simulate behaviors similar to those of cold-pool outflows in atmospheric convection, including open cell formation.

In Bengtsson, Bao, et al., 2019, a CA was used in the Chikira and Sugiyama (2016) convection scheme which assumes a subgrid spectral representation of plumes. Thus, the subgrid plume population provided by the CA could be directly tied to the number of plumes used in the convection scheme. In this study, the CA is implemented in the NOAA UFS at ~25 km horizontal resolution, with model physics from the operational GFS (2020) (GFSv15.1), which uses the currently operational "Scale Aware Simplified Arakawa Schubert" (SASAS) cumulus convection scheme (Arakawa & Schubert, 1974; Han et al., 2017; Han & Pan, 2011; Pan & Wu, 1995). The SASAS is a bulk mass-flux scheme described using an entraining-detraining single-plume model. Thus, the subgrid organization provided by the CA is used in terms of either area coverage, plume radius or triggering of nearby convection similar to the "org" scheme proposed by Mapes and Neale (2011).

The CA used in this study is an extension to the automaton family known as "Generations," which in turn is based on the "Game of Life" (Chopard & Droz, 1998) but adds cell history to the rule set. It is a deterministic CA ruleset, initialized with Gaussian white noise. Thus, when used in an ensemble system, each ensemble member can provide a different seed to the random number generator governing the initial state to then generate a different evolution for each member. By cell history we refer to newborn cells being given a "lifetime,"τ, that is incrementally reduced by 1 each time step where the rules are not met, in contrast to going directly from 1 to 0. Similar to the method in Bengtsson et al. (2013), the CA is conditioned on a forcing from the NWP model through the lifetime variable τ such that:

$$\tau = N\left(\frac{\int_{l=1}^{l=\text{top}} E\frac{dp}{g}}{\max\left(\int_{l=1}^{l=\text{top}} E\frac{dp}{g}\right)}\right) \tag{1}$$

here, N is an integer that when multiplied by the model time-step represents a physical time scale, such that τ is longer in regions where the forcing is larger, E is the convective rain evaporation. The denominator is the maximum value of the forcing in the global domain. While the grid-scale forcing in practice could be any two-dimensional field, we choose here to set it as the vertically integrated subgrid rain evaporation amount, serving as an indicator of geographical regions where enhanced subgrid organization may arise through convective cold-pools.

Figure 1 shows a flow-chart of the proposed organization scheme, following the schematic outlined in Figure 1 of Mapes and Neale (2011). The large scale forcing that drives the CA evolution is subgrid rain evaporation, and a stochastic initial plume-distribution is prescribed, resulting in different subgrid organization in each realization (ensemble member). Also shown in Figure 1 is a crude snap-shot of a schematic image of the CA grid (blue grid) overlaid on the NWP model grid (gray). Black cells indicate a CA state that is active, whereas light blue cells indicate a CA state that is inactive. After the CA is updated, we count the number of plumes (represented by connected CA cells), and their associated size within each NWP grid-box, and couple them to the convection scheme as described below. As an example, the largest cluster of cells found on the subgrid in the grid-box that is outlined with red lines is of size five cells. The upper right panel in Figure 1 shows what the CA can look like in the UFS, when conditioned on the convective rain evaporation, here first coarse grained to the NWP model grid of ~25 km resolution, and then further coarse grained to a 1×1 degree grid.

Using the above approach, we carry out the following sensitivity tests:

- Entrainment: In entraining plume model bulk mass-flux schemes, the upward mass-flux is typically parameterized as a function of environmental air being entrained into the rising plume (as well as parcel

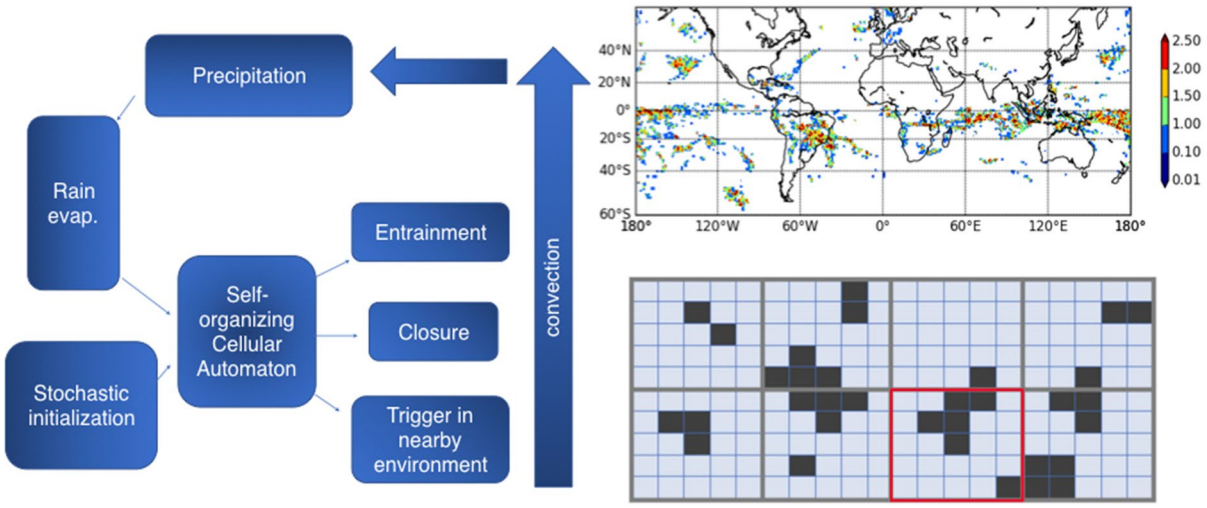

Figure 1. Left: Flow-chart illustrating the convective organization scheme, adapted from Figure 1 in Mapes and Neale (2011). Bottom right: schematic illustrating a possible snap-shot of the cellular automaton evolution, black cells indicate active cells, blue cells indicate inactive cells (Bengtsson, Bao, et al., 2019, © American Meteorological Society. Used with permission). Thin blue line represents the cellular automaton grid, whereas the dark gray lines indicate the NWP model grid. Top right: a snap-shot of the cellular automata pattern from the UFS first coarse-grained to the ~25 km grid, then further gridded to a 1 × 1 degree output field. Values represent the number of cells in the largest connected plume. NWP, numerical weather prediction; UFS, Unified Forecast System.

properties at cloud base). The fractional entrainment is described as a function of the plume radius (from laboratory water tank experiments of thermal plumes—Morton et al., 1956; Turner & Yang, 1963). Larger thermals (plumes) have smaller fractional entrainment, which is a consequence of the fact that larger areas have relatively smaller perimeters. In this study, the assumption is that subgrid organization will lead to a few larger plumes rather than several smaller plumes, such that the grid-box average fractional entrainment is reduced. Thus, after the CA is updated, we count the number of plumes (represented by connected CA cells—Figure 1), and their associated size within each NWP grid-box. If the largest cluster of cells found on the subgrid is larger than a set radius, then the fractional entrainment rate is reduced at that grid-point by 30% (selected based on experimentation)

- Triggering: In NWP models physical processes are parameterized in columns, and the horizontal interaction between physical processes takes place only through advection and diffusion. As the CA can organize clusters across adjacent NWP model grid-boxes, the method offers a novel approach to enhance the probability of triggering of convection in nearby areas, representing subgrid fluctuations in temperature and humidity, and triggering in premoistened regions if convection is triggered in a cluster. The stochastic nature of the CA may enhance organization in different directions within the grid-box, and across grid-boxes, depending on the initial seed. If the model is run as an ensemble, the convection scheme's stochastic triggering function can help to improve uncertainty estimates associated with subgrid fluctuations of temperature and humidity and randomness in organization. In this work, model grid boxes in which the CA's largest connecting plume exceeds a given threshold will be considered as candidates for convective activation, in addition to the scheme's current triggering criteria
- Closure: We assume that convection that organizes into plumes with larger radii tends to cover a larger area fraction of the grid-box and thereby acts to enhance the cloud base mass flux. This idea is in line with the methodology outlined in Bengtsson et al. (2013), with the difference being that the convection scheme in that study utilized a prognostic equation for the updraft area fraction, such that the CA area fraction could be used as a source term. In this coupling strategy, we again count the number of plumes (represented by connected cellular automaton cells—Figure 1), and their associated size within each NWP grid-box. If the largest cluster of cells found on the subgrid is larger than a set radius, then the cloud base mass-flux is enhanced in that grid-box by 25% (selected based on experimentation)

In this study, the CA grid is 5 × 5 times the resolution of the NWP model grid, while the threshold value used to determine when to apply the coupling discussed above is set through trial-and-error to a cluster size

of eight cells. This value is the same regardless of coupling the CA to the closure, entrainment or triggering. The integer controlling the time-scale N was again set through trial-and-error to 25 for the trigger and closure formulations, and to 50 for the entrainment formulation. A lower threshold value, and/or a larger time-scale value both result in stronger deep convection, and in the case of CA_trigger, convection activated in more grid-points. It is worth emphasizing that the CA scheme outlined here functions, similarly to Mapes and Neale (2011), as a positive feedback on deep convection development through enhanced subgrid organization. While the CA scheme stochastically selects the points to be enhanced (together with the large-scale condition), the scheme does not provide a symmetrical perturbation to a state, tendency, or parameter as is commonly the assumption in stochastic parameterizations (e.g., those listed in the review paper on stochastic parameterizations by Berner et al., 2017).

2.2. Stochastically Perturbed Physics Tendencies

As outlined in Buizza et al. (1999), the SPPT scheme is designed to represent model uncertainty due to physical parameterizations by perturbing the net tendencies from the various physical parameterizations represented in the model by multiplicative spatially and temporally correlated noise. In this study, we are interested in seeing how our stochastic convection parameterization compares to the methodology of perturbing the output tendencies with multiplicative noise. Since we are only considering deep cumulus convection in this study, we compare our development with SPPT perturbations on tendencies that are produced by the deep convection scheme (contrary to the total physics tendency), and we use spatial correlation scales of 500 km and temporal correlation scales of 6 h, which are the shortest correlation scales used in the SPPT scheme in the operational NOAA Global Ensemble Forecast System v12 (GEFS).

2.3. Data—The Numerical Model

The configuration of the UFS used here is close to that currently used in NOAA operations, where the effects of ocean-atmosphere coupling are neglected and the suite of model physics are defined by the tag GFSv15.1. The dynamical core is the finite volume cubed-sphere (FV3), which is described in S. Lin and Rood (1996), S. Lin (2004) and Harris et al. (2016) and references therein. The PBL scheme is that described in J. Han and Pan (2011) and J. Han et al. (2016), which uses an eddy diffusion mass flux parameterization where the mixing by eddy diffusion is modeled by a so-called eddy-diffusivity counter-gradient mixing (Hong & Pan, 1996; Troen & Mahrt, 1986), and the mixing by convective plumes is modeled using a mass flux approach, following Siebesma et al. (2007). The cloud microphysics is a one-moment bulk scheme using six prognostic water species (mixing ratio); vapor, liquid, ice, rain, snow, and graupel referred to as the GFDL cloud microphysics scheme (Chen & Lin, 2013; Y. L. Lin et al., 1983). The shallow and deep cumulus parameterization are variants of the simplified Arakawa-Schubert (SAS) scheme described in Pan and Wu (1995), J. Han and Pan (2011) and J. Han et al. (2017), where closure assumptions are based on quasiequilibrium theory.

2.4. Data—Observations and Reanalysis

Precipitation forecasts are verified against precipitation estimates from the Tropical Rainfall Measuring Mission 3B42 product (TRMM; Huffman et al., 2007) and the bias corrected Climate Prediction Center morphing technique product (CMORPH; Joyce et al., 2004). Both data sets are available on a 25-degree grid and 3 hourly temporal resolution and were re-gridded to match the FV3GFS output. For evaluation of some dynamical variables and precipitation, the ECMWF ERA interim reanalysis data were used (Dee et al., 2011).

3. Experiment Design

All model simulations use a horizontal resolution of C384 (~25 km resolution along the equator), 65 vertical levels, and a model physics timestep of 450 s. The initial conditions for the atmosphere, land surface and sea surface temperature (SST) come from a preoperational run corresponding to GFSv15, and SST's are relaxed to a climatology on a time-scale of 90 days to account for seasonality. To study precipitation organization, we carry out 30 day forecast with 3-hourly output on the 25 km grid in single stochastic runs. For

the analysis of tropical variability, we carry out seasonal, 90-day forecasts in a 20 member +1 unperturbed control ensemble generated by initial condition perturbations for the reference run starting at the initial time January 30, 2016 00 UTC. For the CA runs, we use 20-member initial condition perturbations plus a different seed in the random number generator. In the following sections, the different couplings to the convection scheme are referred to as CA_entr, CA_trigger, and CA_closure for entrainment, triggering, and closure applications respectively.

4. Results

4.1. Spatial and Temporal Convective Organization

First of all, we intercompare the different CA configurations' ability to organize tropical precipitation by computing the spatial autocorrelation and autocovariance of precipitation, as well as precipitation duration following the methodology outlined in Ricciardulli and Sardeshmukh (2002). For this purpose, we use model output and observational (TRMM) data at 25 km grid-spacing, with 3-hourly temporal resolution in single stochastic 30-day forecasts. The precipitation organization metrics are presented in Figure 2. Figures 2a and 2b show the spatial autocorrelation and autocovariance respectively, computed between 15°S and 15°N. In general, the spatial autocorrelation is higher in the model simulations than in the observations, this may be attributed to more persistent drizzle precipitation in the model. The CA_trigger configuration is the only configuration that notably impacts the spatial autocorrelation, bringing it closer to the observations as a result of more deep convective points being triggered where the control forecast has more drizzle like precipitation. Since we are mainly interested in deep convection, in order to avoid the implications of drizzle contamination in the statistics, we next look at the autocovariance, which provides information on both persistence and amplitude of the variations. The spatial autocovariance is increased as a result of the CA updates bringing the autocovariance closer to the observations, and the largest improvement in this metric can be found when the CA informs about convective initiation (CA_trigger).

Next, we look at the duration of deep convective events following the methodology outlined in Ricciardulli and Sardeshmukh (2002). In our study, a deep convective event is defined as the 3 hourly average precipitation rate >2.5 mm/h. At each grid point, the probability density function $P(t_c)$ of deep convective durations, t_c, was estimated through histogram analysis. As an example Figure 2c shows the expected mean value $\bar{t}_c = \Sigma\, t_c\, P(t_c)$ of the modeled control forecast in each grid-point. Although our data set is smaller than the one used in Ricciardulli and Sardeshmukh (2002), the geographical distribution of deep convection durations, as well as the mean duration compares well with their long-term observational data. Figure 2d shows the histogram of the ocean points in Figure 2c for both observational data (TRMM) and the model simulations. While the impact on the deep convective duration is small, the CA_trigger configuration reduces the frequency of long durations, and increases the frequency of short durations to yield a distribution which corresponds better with the observed duration of deep convective precipitation. Taken together, the results in Figure 2 suggest that the CA scheme in general, and the CA_trigger configuration in particular, enhances the organization of deep convection by initiating new convection in neighboring grid-points where subgrid rain evaporation is strong, introducing three-dimensional effects.

4.2. Hovmöller Diagrams and Radon Projection

Comparing the models' mean state of precipitation (ensemble average) to TRMM satellite precipitation observations suggests that the CA-based parameterizations of convective organization generally have a very small impact on the mean state (not shown). The modifications do not introduce any significant biases compared with the reference run, but it is also difficult to conclude if the CA-based parameterizations are associated with any substantial improvement in the mean state either. Because tropical variability is known to be influenced by the basic state (e.g., Dias & Kiladis, 2014; Han & Khouider, 2010; Tulich & Kiladis, 2012; Zhang & Webster, 1989), the fact that the mean precipitation pattern is not strongly influenced by the introduction of the CA is considered to be a desirable feature of the modified schemes. We first examine Hovmöller diagrams (Hovmöller, 1949), to assess whether the model can generate CCEW variability far from its initial state and to understand how the modified parameterizations affect the behavior of convective organization and propagation. The Hovmöller diagram for the observed (90 day) precipitation averaged over

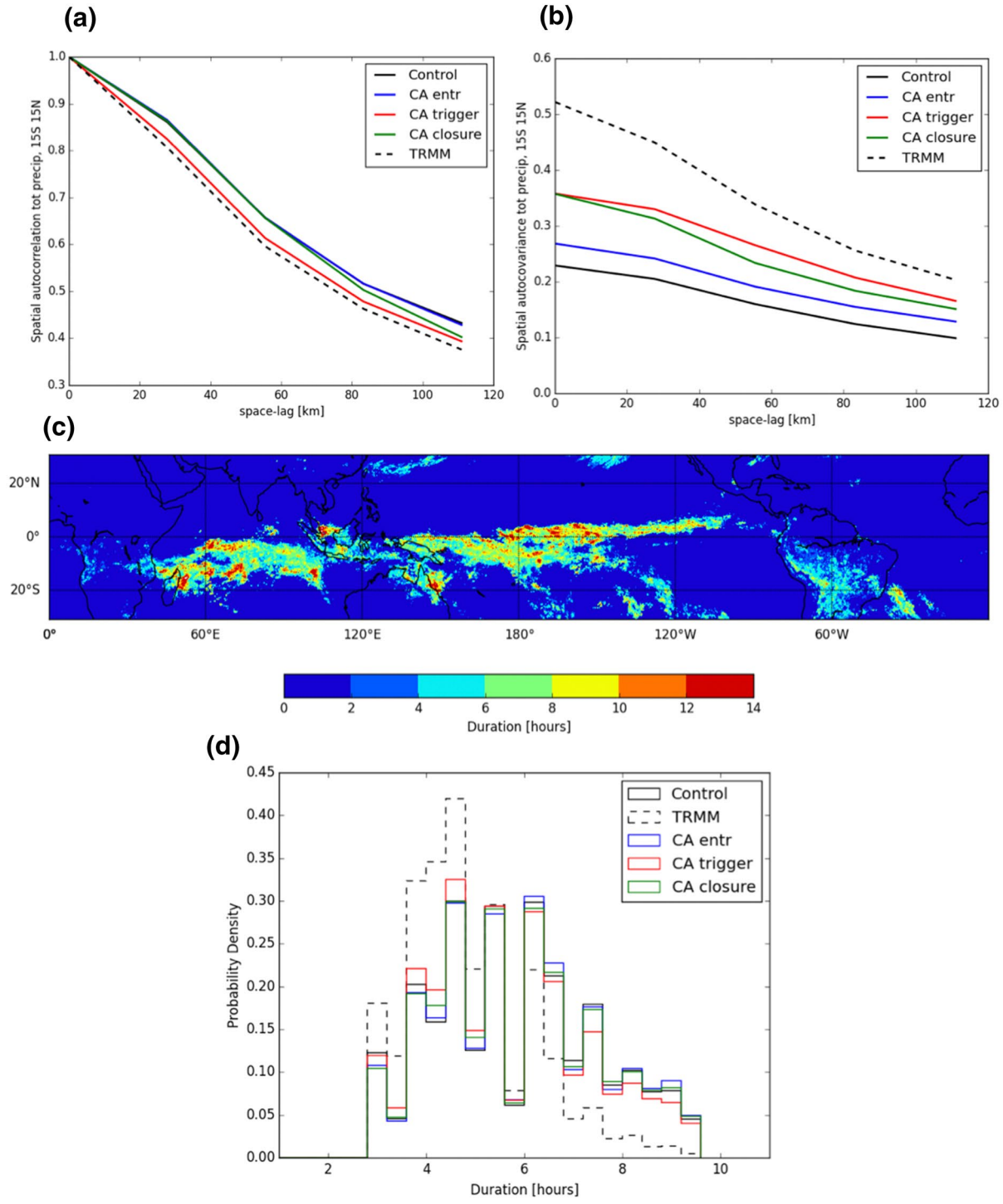

Figure 2. (a) Spatial autocorrelation of total precipitation, (b) Spatial autocovariance of total precipitation (c) Expected mean Probability Density Function (PDF) of deep convective precipitation duration [hours], (d) Histogram distribution of the expected mean PDF as plotted in (c) [hours]. Solid lines are modeled precipitation in different configurations, dashed lines are observations.

the Tropical band 5°S to 5°N in Figure 3 illustrates how precipitation in the tropics tends to be modulated by CCEWs on various time and space scales, with the latter propagating at a range of different phase speeds, both eastward and westward. For instance, during the period of interest, two particularly prominent types of eastward-moving disturbances can be seen in the observations. The first is an MJO event that propagates

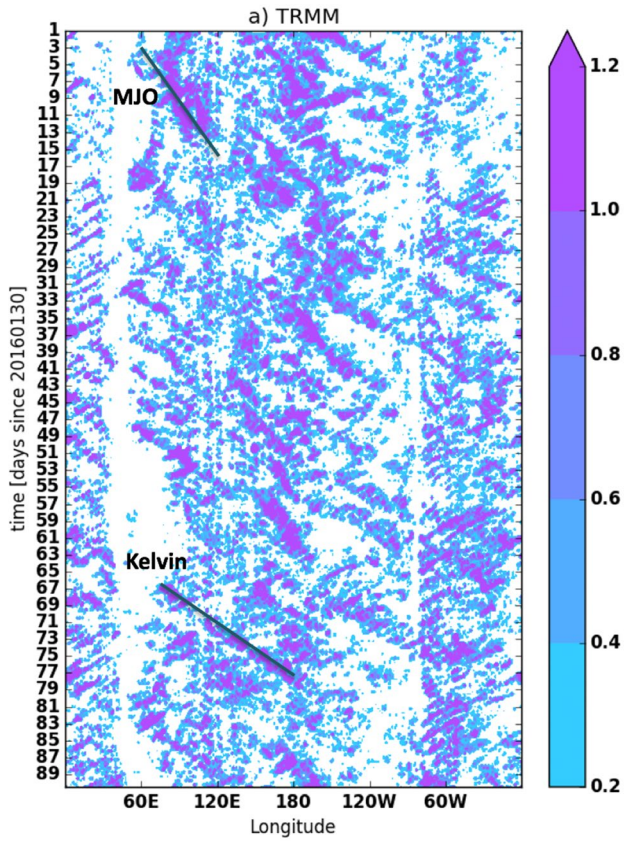

Figure 3. Observed (TRMM) Hovmöller diagram of precipitation (mm/h) for the period 20160130–20160429 between 5°S and 5°N. Lines indicate typical phase speeds associated with MJO (~7 m/s) and Kelvin wave (~15 m/s) propagation. TRMM, Tropical Rainfall Measuring Mission.

eastward at 5–7 m/s across the Indian Ocean and west Pacific during the initial 30 days. The second are convectively coupled Kelvin waves that propagate eastward with a phase-speed of about 15 m/s and are the dominant synoptic features over the central and eastern Pacific, where SSTs happen to be warmer than normal during this period as part of a large-amplitude ENSO event. The organization and propagation of CCEWs in the forecast model simulations is markedly unpredictable, both in terms of amplitude and variance, as well as the phase speed of individual disturbances. This lack of predictability is illustrated in Figure 4, where the Hovmöller diagrams of the first three ensemble members from the reference configuration are shown. Recall that the ensemble members are made to differ only through the use of different initial condition perturbations. The MJO event at the initial time of the simulation is forecasted with some resemblance among the three different ensemble members, but after about 30 days, differences become substantial and there is generally less evidence of propagation with increasing lead time as compared to observations. This same general evolution is apparent in the remaining 17 ensemble members (not shown).

Comparing individual realizations from the various CA and SPPT integrations in Figure 5, the diversity of behaviors is also seen to be quite large, and thus it is challenging to determine from these Hovm ller diagrams whether the use and choice of CA coupling leads to any systematic differences in the nature of tropical convective wave organization. Nevertheless, the CA-based schemes generally appear to provide some enhancement in precipitation variance and propagation as compared to the SSPT scheme as well the reference integrations in Figure 4, especially in the case of the CA_trigger application, where enhanced eastward propagation can be seen over the Pacific Ocean (120°E to 120°W) for longer forecast lead times (e.g., after 30 days).

To quantify this diversity in behavior across ensemble members and CA configurations, we first look at the pattern correlation between the

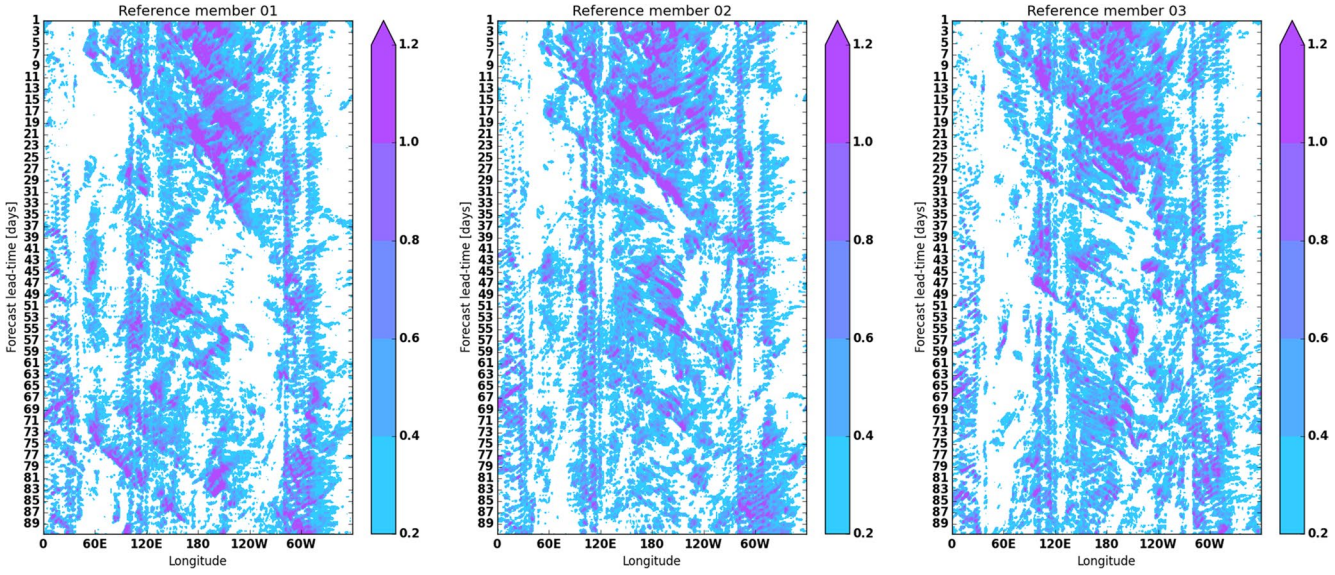

Figure 4. Hovmöller diagram of precipitation (mm/h) for the period 20160130–20160429 between 5°S and 5°N, for the three first members of the Reference UFS model simulation, the different realizations are only due to different initial condition perturbations. UDS, Unified Forecast System.

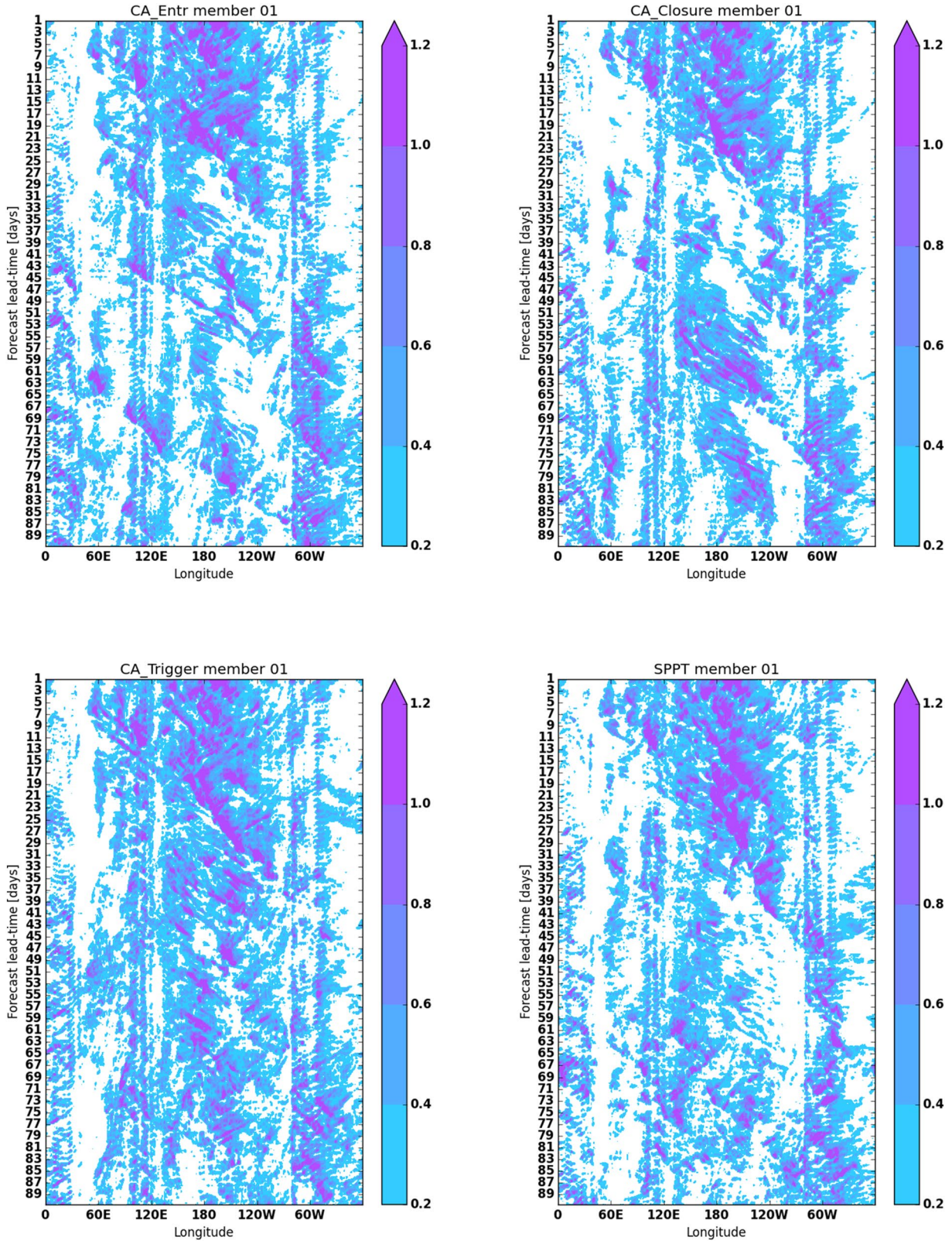

Figure 5. Hovmöller diagram of precipitation (mm/h) for the period 20160130–20160429 between 5°S and 5°N, for member 1 from the CA_entr, CA_closure, CA_trigger and SPPT model simulations. CA, cellular automata; SPPT, Stochastically Perturbed Physics Tendency.

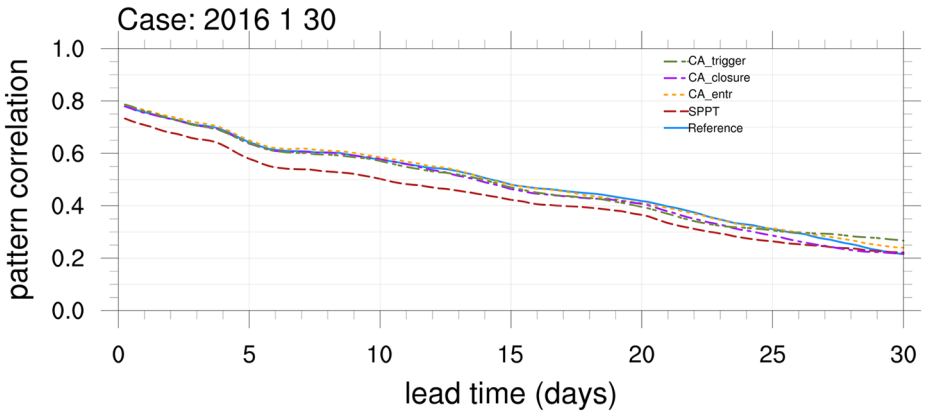

Figure 6. Pattern correlation (in time and longitude) for precipitation averaged from 5°S to 5°N using each ensemble member as control and then averaging across all 20 ensemble members. Pattern correlation is computed for 7 day running windows at each forecast hour.

ensemble members of the Hovmöller diagrams, which also helps us understand if there is any "potential skill" obtained from the new parameterizations. We compute the centered pattern correlation of latitude averaged forecast precipitation among different ensemble members at each lead time. Each ensemble member is in turn considered the "truth" and correlated with all other ensemble members and the resulting correlation coefficients are then averaged. This is done to ensure against potential outlier ensemble members decreasing the correlation artificially. This procedure is also done using TRMM precipitation as the "truth" and the results give generally lower correlations, but similar overall results. Figure 6 suggests that while no added potential skill in pattern correlation is found in the CA model runs, perturbing the tendency produced by the convection scheme with correlated random noise, as in SPPT, degrades the potential skill of the Hovmöller pattern correlation. This is not solely due to increased ensemble spread, as the ensemble spread of the pattern correlation is equally large for the Reference, SPPT and CA simulations (not shown). Importantly, this potential skill analysis indicates that the initiation and propagation of the disturbances is highly unpredictable, and large spread can be seen among the ensemble members. For these reasons, here, we are more interested in the statistics of the model's ability to organize disturbances, rather than getting the exact time and location correct, and we are also interested in determining whether one method of the CA configuration is better than another in a statistical sense.

To make such statistical assessment of the various model configurations, another convenient way of summarizing the information provided by Hovmöller diagrams is to construct so-called Radon projections (Deans, 1983), which convey the distribution of variance as a function of propagation speed for the field of interest. The methods used to construct these diagrams are detailed in G. Y. Yang et al. (2007) and Dias and Pauluis (2011). Briefly, when a line in the longitude-time domain is perpendicular to the crests and troughs of a wave, the energy of the projected data along this line has a maximum, and hence the angle perpendicular to the projection gives the wave propagation direction and, thus, the phase speed. Here, the precipitation forecast data are first averaged in the meridional direction from 5°S to 5°N, then the 90-day forecast is split into 15-days window spanning all longitudes, with a 1-day sliding start day. The Radon transform is applied to each of these longitude-time subsets, which yields the projected data along lines at each angle from 0° to 180° in the (longitude, time) plane. For a particular forecast lead period, the dominant zonal phase speed of precipitating features corresponds to the mean peak in energy calculated including each Hovmöller subset within that lead period. We note that while the peak location is robust to our choice of 15-days window, the spread about this peak tends to increase with increasing window length (not shown). The Radon projections plotted from day 20 to day 90 in Figure 7 nicely capture the observed peak in the TRMM and CMORPH data (two gray lines) of the phase speeds associated with convectively coupled equatorial Kelvin waves (~15 m/s). In Figure 7a, these observations are compared to the unperturbed control forecast (black line). Owing to random chance, this unperturbed control run has the lowest variance of all the members and shows almost equal variance in both the eastward and westward direction. In Figure 7b the Radon spectra for various ensemble members in the reference case (with only perturbed initial conditions) are also plotted.

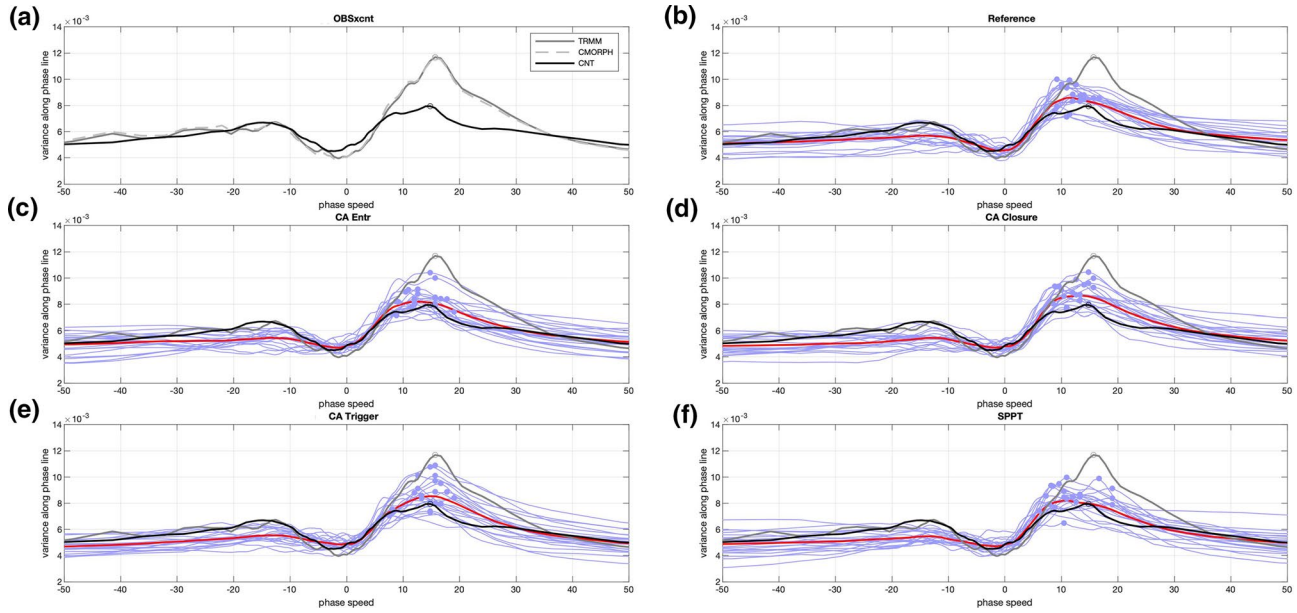

Figure 7. Radon projection plots for days 20–90 between 5°S and 5°N (see text for details). Thin blue lines represent the ensemble members, red lines their average, the thick black line is the unperturbed control and the gray lines are observations (TRMM—solid, CMORPH dashed). The filled circles indicate the phase speed of the maximum variance detected in each member. The Radon projection is shown for (a) Observations/control (b) Reference, (c) CA_entr, (d) CA_closure, (e) CA_trigger and (f) SPPT. CA, cellular automata; CMORPH, Climate Prediction Center morphing technique product; SPPT, Stochastically Perturbed Physics Tendency; TRMM, Tropical Rainfall Measuring Mission.

The ensemble members generally show a bias toward eastward versus westward propagation, (unlike in the unperturbed control forecast), although the eastward peak is systematically slower and much weaker than observed. Figures 7c and 7d shows the ensemble members (blue lines), and their average (red lines) of the three CA applications, CA_entr, CA_closure, and CA_trigger respectively. The distributions in each case show an enhancement in eastward versus westward propagation as well as a shift toward faster phase speeds bringing the model closer to the observed peak at ~15 m/s. Compared with the observations, the CA_trigger application shows the greatest improvement relative to the reference case in terms of eastward precipitation variance and propagation speed. In the SPPT runs (Figure 7e), while some members exhibit an increase in propagation speed, others show reduction, such that there is no systematic change in the distribution. These results are promising in the sense that they suggest that the stochastic CA scheme can improve the propagation speed of Kelvin waves in a more systematic manner than random multiplicative noise. Therefore, our convective parameterization approach is potentially beneficial for the model's ability to reproduce the observed large-scale organization of convectively coupled tropical variability.

While the Radon transformation is a convenient technique for assessing changes in precipitating features propagation speeds, it does not capture how the different convective scheme configurations might affect Kelvin waves spatial scale, or the strength of the coupling between dynamics and moist convection. One way to address these two issues is to compute the longitude-time coherence-squared and phase spectra between dynamical fields and precipitation. We follow the methodology from Dias et al. (2018) and Bengtsson, Bao, et al. (2019) to calculate the two-dimensional spectra where each 90-day forecast is split into 46-day segments overlapping by 20 days. Longitude–time cross spectra are computed for each segment and at each latitude from 15°S to 15°N. Spectral coefficients are then averaged over latitude and, for the model runs, over the 20 ensemble members. Those spectral coefficients are then used to estimate the coherence-squared and phase (Wheeler & Kiladis, 1999). This technique shows that, in 40 years of reanalyzes, there is high coherence-squared along the equatorial wave theoretical dispersion curves (Wheeler & Kiladis, 1999) between ERAi 850 hPa divergence and precipitation, including the region corresponding to Kelvin waves, which can be found along the dispersion curve marked with "Kelvin" in Figure 8. In addition, the arrows pointing downward and to the right around the Kelvin wave dispersion curve indicate that 850 hPa convergence leads precipitation. Here, we use this diagram as a benchmark for the statistical model performance

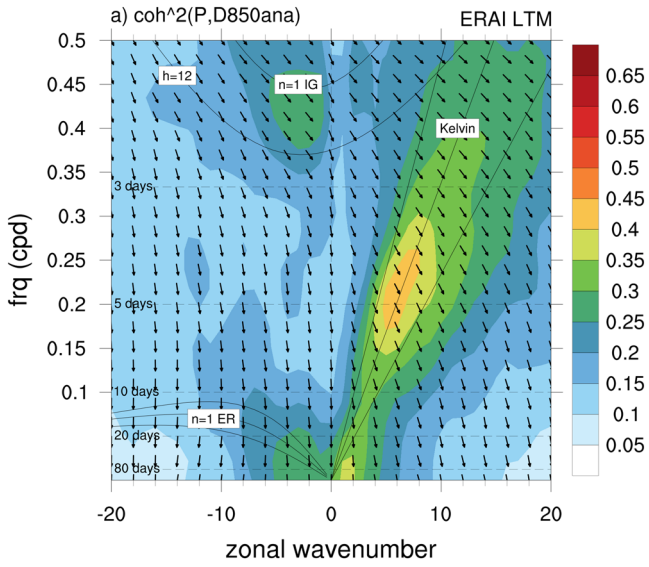

Figure 8. Zonal wavenumber—frequency coherence-squared spectrum between ERAI 850 hPa divergence and precipitation between 15°S and 15°N for 20 February—April 30, 1979–2018. Contours show coherence-squared values, arrows show the phase vectors. Phase vectors pointed up show an in-phase relationship, arrows pointing down mean an out of phase relationship and arrows to the right are for precipitation leading divergence, arrows to the left are precipitation lagging divergence. Coherence-squared values are significant at the 90% level. Lines are the theoretical dispersion curves for the linear shallow water solutions.

with respect to Kelvin Waves. We note that while coherence values can slightly vary across reanalysis datasets and satellite estimates of precipitation, comparison of previous studies suggest that the patterns shown in Figure 8 are robust (Bengtsson, Bao, et al., 2019; Kim & Alexander, 2013; Wheeler & Kiladis, 1999).

All panels in Figure 9 are similar to Figure 8, except that they are computed using only data corresponding to the last 70 days of the model runs. Comparing Figure 9 to Figure 8 shows that while the observed Kelvin wave spectral characteristics can be seen using a single 70 days period, coherence is, not surprisingly, noisier. In the model simulations the coherence between 850 hPa convergence and precipitation is a lot larger compared with reanalysis, in particular in the lower frequency waves. Notably, the SPPT model run enhances the coherence of all wave-modes compared with the reference configuration, suggesting too strong coupling between dynamics and precipitation in this case. One explanation for this is that some members of the ensemble will have reduced convective heating/moisting tendencies, which will result in enhanced resolved convection (precipitation driven by the dynamics). The CA_trigger configuration, which had the largest impact on the Radon projection, is also the one configuration with the largest impact on the Kelvin wave spectral characteristics. In particular, CA_trigger is associated with a decrease in coherence in comparison to the reference, with patterns more consistent with reanalysis than in all other setups. It can also be seen that the coherence is reduced for the westward propagating equatorial Rossby waves in the CA_trigger configuration, also consistent with the reanalysis for the given period. The CA_closure and CA_entr model runs don't show a notable impact on the coherence spectra compared with the reference. One possible explanation for the decrease in the coherence spectra seen with the CA_trigger simulation is that in this configuration convection can be initiated in grid-boxes solely determined from the enhanced organization provided by the CA, which may be decoupled from the large-scale dynamics.

4.3. Gross Moist Stability and Vertical Heating Profiles

In order to understand why the phase speed of the eastward propagating convectively coupled Kelvin waves increases with the CA scheme activated, we next study the relationship between convective cloud systems and large-scale dynamics using the concept of gross moist stability (GMS) first introduced by Neelin and Held (1987), and the impact on the vertical heating profiles, as these two concepts have been shown to influence the Kelvin wave phase speed through interaction between latent heat release and with low level moisture convergence (e.g., Fuchs et al., 2012; Wang & Chen, 1989). GMS represents the efficiency of moist static energy export by convectively induced large-scale circulations; thus, by linking convective intensity (defined as vertically integrated moisture flux convergence) with atmospheric processes that regulate column moist energy (defined as vertical and horizontal components of moist entropy divergence), GMS represents a valuable concept that can be used to diagnose organized tropical precipitation (Benedict et al., 2014). The quantity has been used in many theoretical and/or reduced-complexity model studies (e.g., Raymond & Fuchs, 2009; Sugiyama, 2009; A. Sobel and Maloney, 2012, 2013). The relevance of the gross moist stability to equatorial waves in the real atmosphere is not completely established, although some insights have been obtained using observational data (e.g., Inoue & Back, 2015a, 2015b) and General Circulation Models (GCM's) (e.g., Frierson et al., 2011; Hannah & Maloney, 2011, 2014; Benedict et al., 2014). In Raymond et al. (2007) and Fuchs and Raymond (2007), a quantity called NGMS was defined, which is the ratio of column moist static energy advection to intensity of the convection. In the literature, slightly different definitions of NGMS can be found, and it is sometimes interchangeably used with just "GMS" (e.g., Benedict et al., 2014; Fuchs and Raymond, 2007; Raymond et al., 2009; Raymond & Fuchs, 2009; Sugiyama, 2009). Importantly, the physical implications between the different definitions are consistent as NGMS represents

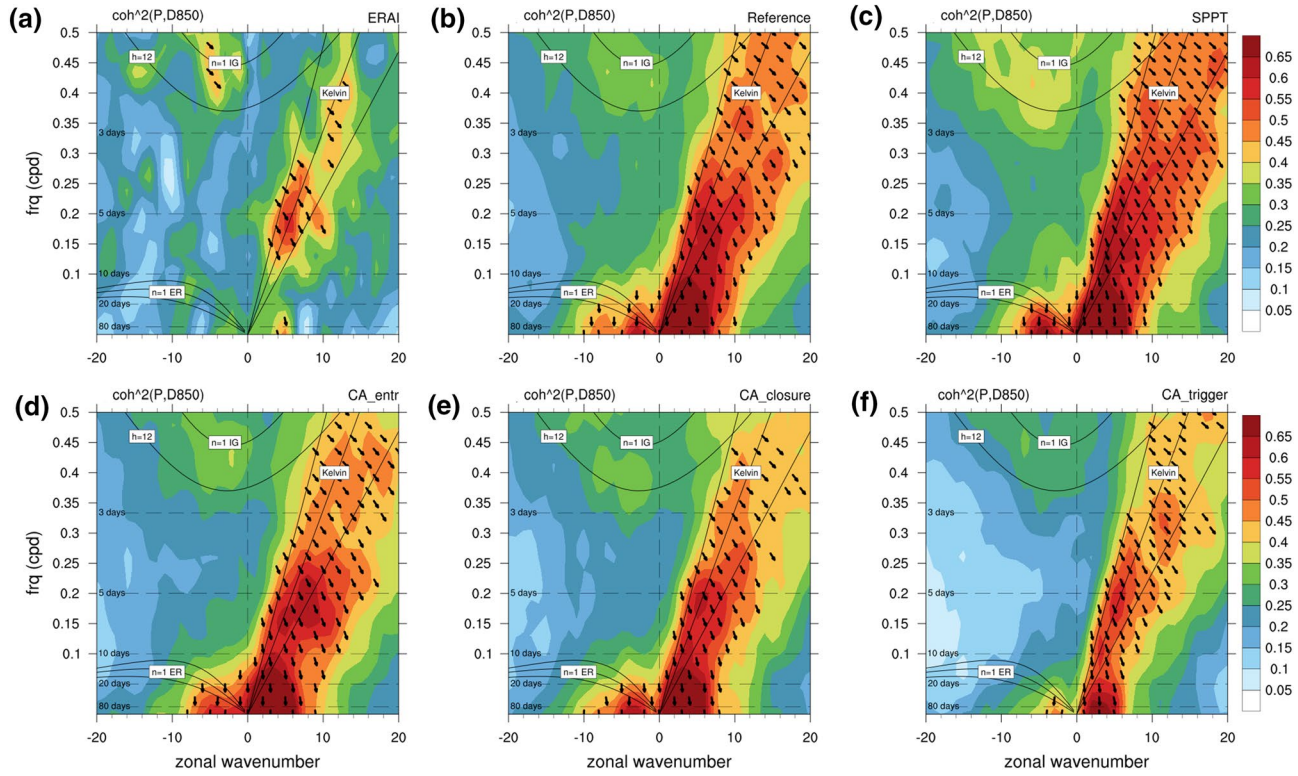

Figure 9. Zonal wavenumber—frequency coherence-squared spectrum between 850 hPa divergence and precipitation between 15°S and 15°N for 20 February—April 30, 2016. Panel (a) ERAI 850 hPa divergence and precipitation, panel (b–f) model forecast 850 hPa divergence and precipitation for the different experiments: (b) Reference forecast, (c) SPPT, (d) CA_entr, (e) CA_closure, and (f) CA_trigger experiment. Contours are coherence-squared values, arrows the phase vectors. Phase vectors pointed up show an in-phase relationship, arrows pointing down mean an out of phase relationship. Arrows to the right are for precipitation leading divergence, arrows to the left are precipitation lagging divergence. Coherence-squared values are significant at the 90% level. CA, cellular automata; SPPT, Stochastically Perturbed Physics Tendency.

the efficiency export of a quantity conserved in moist adiabatic processes, per unit intensity of the convection (Raymond et al., 2009).

The role of NGMS on Kelvin wave phase speed was studied in a reduced-complexity GCM in Frierson (2007). They found that when changes were made to a convection scheme parameter that controls the fraction of convective versus large-scale precipitation to enhance large-scale precipitation, the waves increased in strength, propagated more slowly, and moved to larger scales. They further showed that this decrease in phase speed was found to be related to a reduction of GMS of the atmosphere, which was reduced with increased large-scale precipitation. Their findings suggest that large-scale precipitation is not very effective at stabilizing the atmosphere, whereas when the convection scheme is more active, CAPE is quickly reduced, the upper troposphere is warmer and convection is deeper, leading to an increase in NGMS. In the present study we compare the NGMS of our simulations as well as the fraction of convective versus large-scale precipitation to understand if the increase in Kelvin wave phase speed we find can be linked to an increase in NGMS. Since we are doing the computations of NGMS in a relatively high resolution GCM simulation, substantial space-time averaging is required to obtain a statistically stable quantity that can be interpreted in terms of physical mechanisms. For instance, since NGMS is indicative of the stability of the atmosphere only where condensation occurs, we expect the NGMS averaged over the region of upward motion to be most important in determining the wave speed as implied, for instance, in A. H. Sobel and Bretherton (2003), Frierson (2007), and Benedict et al. (2014).

NGMS is derived from the budget of vertically integrated moist static energy, $h = C_p T + gz + L_v q$, and may be written as the total NGMS, Γ_T, which can be further split up into the horizontal and vertical components Γ_H and Γ_V, respectively:

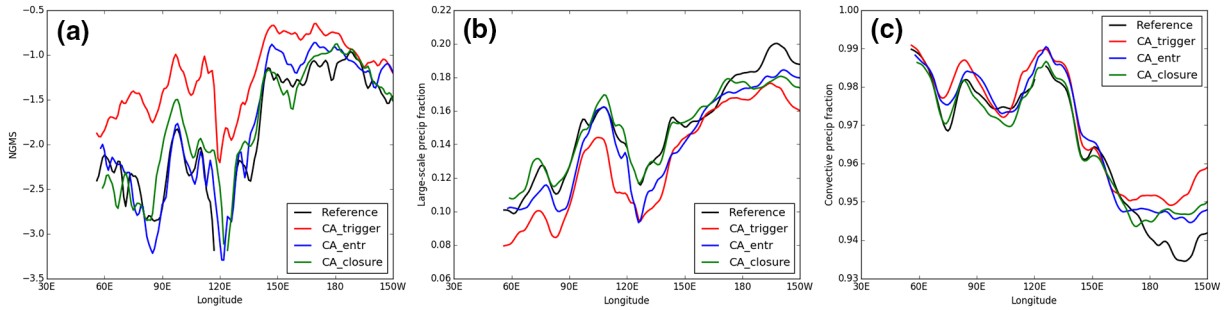

Figure 10. (a) Vertical component of Normalized Gross Moist Stability (NGMS). (b) Large-scale precipitation fraction, and (c) convective precipitation fraction. Variables have been latitudinally averaged over a chosen Indo-Pacific domain where climatological vertically integrated moisture convergence is positive following the methodology in Benedict et al. (2014).

$$\Gamma_T = -\frac{T_R\left[\mathbf{v}\cdot\nabla h + \omega\left(\frac{\partial h}{\partial p}\right)\right]}{L\left[\nabla\left(q\mathbf{v}\right)\right]}, \tag{2}$$

$$\Gamma_H = -\frac{T_R\left[\mathbf{v}\cdot\nabla h\right]}{L\left[\nabla\left(q\mathbf{v}\right)\right]}, \tag{3}$$

$$\Gamma_V = -\frac{T_R\left[\omega\left(\frac{\partial h}{\partial p}\right)\right]}{L\left[\nabla\left(q\mathbf{v}\right)\right]}, \tag{4}$$

here, C_p is the specific heat at constant pressure, T is temperature, g is the gravitational constant, z is the height above the surface, L is the latent heat of vaporization. $\mathbf{v}$ is the horizontal vector wind, ω is the vertical pressure velocity, p is the atmospheric pressure, ∇ is the gradient operator, q is the specific humidity, and $T_R = 273.1$ K. The square brackets indicated vertical integration between the surface and the tropopause.

We next follow closely the method outlined in Benedict et al. (2014) to generate the time-mean and meridionally averaged vertical component of the NGMS shown in Figure 10:

1. The numerator and denominator are vertically integrated separately and then combined to obtain NGMS following Raymond et al. (2009) and Benedict et al. (2014)
2. We apply a 17-day running temporal average and a 5° sliding box smoothing centered at each grid point to the numerator and denominator separately. No land points are included in any spatial averaging
3. Meridional averaging is computed using a dynamic latitude mask that includes only oceanic grid points where time-mean vertically integrated moisture convergence is positive
4. We restrict the latitudinal bounds to be at most 15° from the equator
5. Two passes of a 1-2-1 filter have been applied in longitude prior to plotting
6. Lastly, we select the same period as associated with most of the Kelvin wave activity, days 20–90 as plotted in the Radon projection plots in Figure 7

All the advection and convergence terms are computed at the grid-scale within the model. The final NGMS is shown in Figure 10 for the average over the 20 ensemble members for the Reference (black) and the CA_trigger case (red). It can be seen that the NGMS is quantitatively similar compared to Figure 6 in the Benedict et al. (2014) study, although differences can be seen that are believed to be largely due to the fact that we do not have any MJO events in the data plotted, which was the focus of the Benedict et al. (2014) study. The NGMS in Figure 10 in the present study is dominated by Kelvin wave activity.

As summarized in Raymond et al. (2009), some physical interpretation related to the sign of NGMS can be made in terms of the interaction between convection and large-scale environment, if small temperature variations in the free troposphere are assumed. For instance, negative total NGMS is indicative of convection which results in an increase in column moist static energy, which suggests convection in "build up" stages—such as cumulus congestus or shallow convection (Benedict et al., 2016). On the other hand, positive total NGMS value indicates that convection dries the environment, despite moisture convergence, an indication of deeper cumulus convection. It is difficult to assess whether this interpretation applies to our simulations in a full physics GCM, and as pointed out in Benedict et al. (2016), the vertical component of NGMS has the largest negative values between the total, horizontal and vertical components (Equations 2–4). Thus, we are here more interested in the relative difference in NGMS between the different cases, rather than the exact magnitude of NGMS. Figure 10a suggests that NGMS is generally increased in the CA_trigger application, suggesting a tendency toward more deep convection in this configuration. The impact on NGMS is smaller for the CA_entr and CA_closure configurations.

We next repeat the above steps to plot the convective and large-scale precipitation fraction for the same grid-points, using the same spatial and temporal averaging as for the NGMS. As found in Frierson (2007), Figures 10b and 10c suggests that the speed-up in Kelvin waves in the CA_trigger configuration can partly be attributed to an increase in NGMS as a consequence of increased convective precipitation fraction relative to the large-scale precipitation fraction. The impact on NGMS in the CA_closure and CA_entr runs are less prominent, although in general there is a tendency to larger NGMS values in those configurations as well.

However, as pointed out in Wang and Chen (1989) and Fuchs et al. (2012) the vertical structure of the heating can also modulate wave speeds in addition to the NGMS. As summarized in Fuchs (2015), a top-heavier heating profile results in an unstable Kelvin mode in their simple model, whereas a bottom-heavy heating profile is associated with decaying Kelvin modes. A top-heavy heating profile is also associated with faster Kelvin wave phase-speed, compared with a bottom-heavy profile. Thus, we lastly look at how the different CA couplings impact the heating profiles from the various parameterizations in the model. In Figure 11a, the temperature tendencies from each of the three different CA runs are averaged between 15°S and 15°N. As can be seen, the heating profiles are not impacted by any of the CA schemes, in terms of a bulk tropical average. Figures 11b–11d show the temperature tendencies from each parameterization averaged over points where the CA_entr, CA_closure, and CA_trigger runs respectively are larger than the threshold value for organized plumes (e.g., grid-boxes with eight connecting CA cells in a cluster). The reference run is averaged over the same grid-points as each respective CA coupling run. The net heating profiles (black curves) for these select points are bottom heavy. The impact of enhanced organization from all three coupling strategies gives, per design, more and/or stronger convection, resulting in an increased net heating in these grid-boxes, which shows that the organization representation in the CA scheme results in a positive feedback, similar to the conceptual framework of Mapes and Neale (2011). The net heating profile is enhanced the most in the CA_trigger configuration, with a small tendency to a more bottom-heavy warming, as the net cooling from the microphysics scheme generally takes place in the upper troposphere. In this configuration, convection is not enhanced once triggered, the difference in heating profiles between the CA_trigger run and the reference run is only a consequence of more points in nearby grid-cells having deep convection, or deep convection is triggered in the same grid-cell over a longer time compared with the reference. Compared with the CA_trigger run, the CA_entr run is not associated with any additional latent heat release in the boundary layer, thus, even if modest, in the CA_entr run the change in heating profile is toward a top-heavier profile. Given the small impact on the heating profiles, taken together, Figures 7–11 suggest that a shift (increase) in Kelvin wave phase-speed with the CA scheme can mainly be attributed enhanced NGMS, and the largest shift in phase-speed is found when triggering convection in the nearby environment, or for a longer period, due to enhanced convective organization. For the other two coupling strategies the impact of CA is quite modest, possibly because the changes do not alter where convection is initiated, only how strong the convection will be once it is already triggered.

5. Conclusions

In this study, we investigated the impact of a stochastic convective organization scheme on precipitation organization and CCEWs in the NOAA UFS global weather model. Stochasticity and enhanced organization were modeled using a CA that exhibits self-organizing behavior. Inspired by the organization concept

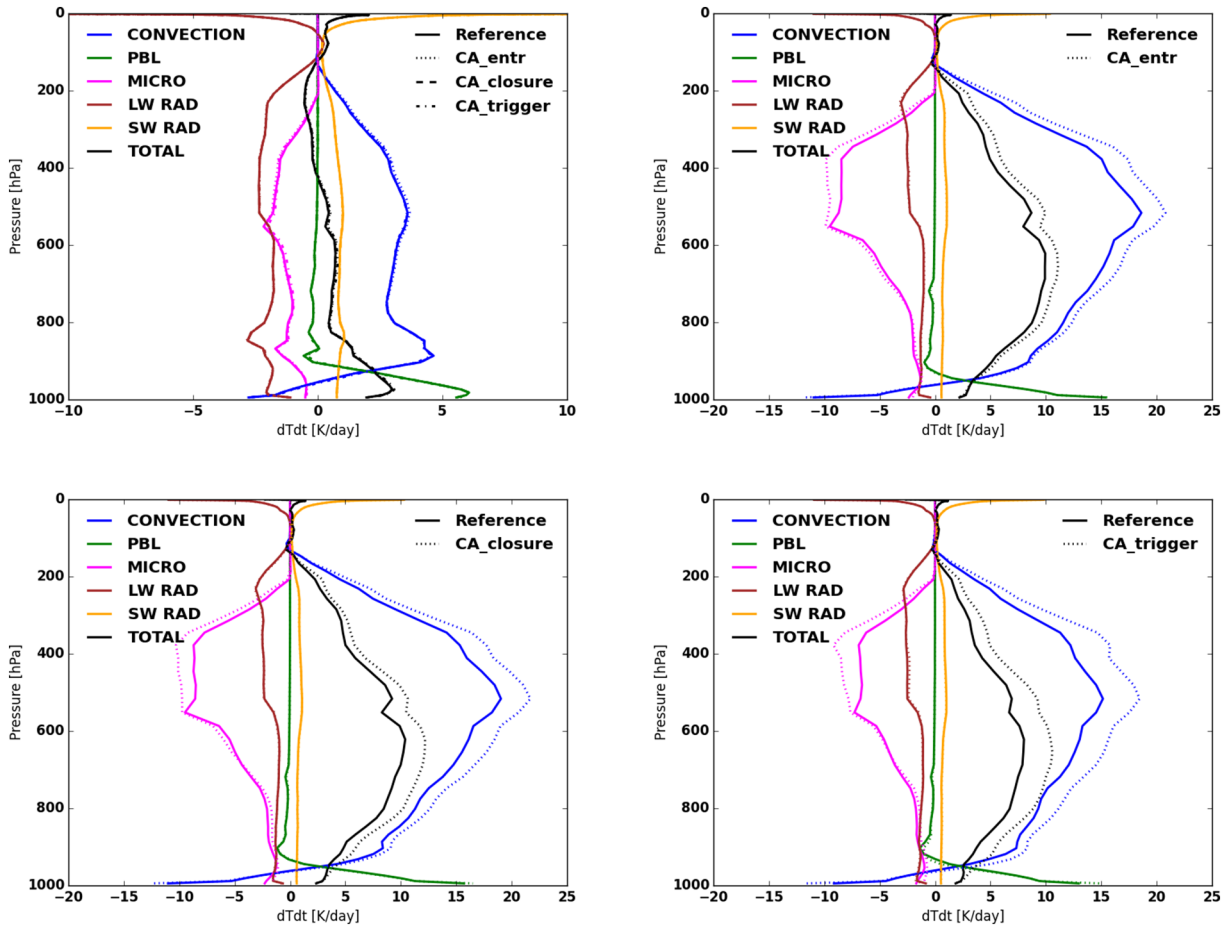

Figure 11. Vertical heating profiles from different physics parameterizations in the model. Top left: Averaged over the 90-day time period, and all longitude points between 5°S and 5°N. Top right and bottom row are averaged over the 90-day period for points 5°S and 5°N where the CA field in the model simulations has a maximum cluster size of at least eight individual CA cells for CA_entr, CA_closure and CA_trigger respectively. CA, cellular automata.

proposed by Mapes and Neale (2011), we studied the sensitivity of coupling the CA to different building blocks of the cumulus convection scheme. This was achieved by enhancing convective activity in regions of increased subgrid organization through changes in triggering, closure and entrainment. The impact of the modified schemes was studied in terms of an assessment of near grid-scale precipitation organization, as well as synoptic scale convective organization in the tropics, and mechanisms of the underlying results were understood by studying the interaction between large-scale moisture and tropical convection. The latter was achieved by employing the concept of GMS, as well as analysis of vertical heating profiles. Furthermore, the impact of the CA scheme was compared with model simulations using the commonly used stochastic physics scheme, SPPT.

One caveat in this study is that the use of the CA is constrained by the fact that the convection scheme, in which the organization is added, is a bulk mass-flux scheme. That is, here it was not possible to take advantage of the full subgrid distribution of CA cells, as was done in Bengtsson et al. (2019). Nevertheless, even in this limited framework, improvements in CCEW phase-speed were found to be related to the increased horizontal communication across NWP grid-boxes using the CA, enhancing stochastic initiation of convection in the nearby environment. Therefore, our study provides some evidence that the proposed CA stochastic organization scheme can be beneficial for the model's ability to improve the observed precipitation organization as well as reproducing the large-scale organization of convectively coupled tropical variability. The main conclusions from our study are:

1. All CA configurations studied here improved the spatial organization of precipitation. The configuration which allows the CA to initiate convection in the nearby environment (CA_trigger) had the largest impact on deep convective spatial and temporal organization, resulting in a spatial autocorrelation and autocovariance of precipitation, as well as deep convective precipitation duration that is closer to the observed scales of organization
2. The CA_trigger configuration also has the largest impact on CCEW between the three different coupling strategies studied here. Specifically, it was found that enhanced convective initiation in the nearby environment provided by the CA in this configuration leads to improvements in the spectral characteristics of equatorial Kelvin waves, and improvements in Kelvin wave phase speed. We showed that the latter is linked to an increase in NGMS—a quantity that represents the efficiency of the advective export of moist static energy by convectively induced large-scale circulations. An increase/reduction of NGMS has been shown to be proportional to an increase/reduction of equatorially trapped wave phase speeds in other studies (e.g., Frierson, 2007; Frierson et al., 2011; Raymond et al., 2009)
3. The stochastic CA scheme provides a more systematic impact on simulated CCEWs, compared with the widely used stochastic parameterization, SPPT. This is not surprising as the CA scheme presented here is designed to let enhanced subgrid (and cross-grid) organization generate a positive convective feedback, whereas SPPT is purely random multiplicative noise. The stochastic initialization of the CA scheme provides opportunities to better capture the full range of uncertainty associated with cumulus convection in the Tropics when used in ensemble forecasting

Future plans include testing our approach in forthcoming versions of the UFS, in particular in the fully coupled UFS, where we would assess the impact of the CA on model uncertainty quantification in the coupled ocean-atmosphere system.

Data Availability Statement

The model output for the Reference and CA configurations used in this study can be accessed here: ftp://ftp2.psl.noaa.gov/Projects/stophy/FV3/CA_runs/. TRMM3B42 can be accessed here: https://disc.gsfc.nasa.gov/datasets/TRMM_3B42_7/summary?keywords=TRMM_3B42_7. CMORPH CRT can be accessed here: https://ftp.cpc.ncep.noaa.gov/precip/CMORPH_V1.0/CRT/0.25deg-3HLY/. ERA interim data can be downloaded here: https://www.ecmwf.int/en/forecasts/datasets/reanalysis-datasets/era-interim.

Acknowledgments
We would like to thank two anonymous reviewers for providing invaluable insight leading to great improvements of our manuscript. We would also like to thank Philip Pegion and Jeffrey Whitaker, NOAA ESRL PSL for helpful NOAA internal reviews. This research was partially supported by the Physical Science Laboratory of NOAA's Earth System Research Laboratory, and by the California Department for Water Resources (CDWR).

References

Ahn, M. S., Kim, D., Park, S., & Ham, Y. G. (2019). Do we need to parameterize mesoscale convective organization to mitigate the MJO-mean state trade-off? *Geophysical Research Letters*, *46*(4), 2293–2301. https://doi.org/10.1029/2018gl080314

Arakawa, A., & Schubert, W. (1974). Interaction of a cumulus cloud ensemble with the large-scale environment, Part I. *Journal of the Atmospheric Sciences*, *31*, 674–701.

Benedict, J. J., Maloney, E. D., Sobel, A. H., & Frierson, D. M. W. (2014). Gross moist stability and MJO simulation skill in three full-physics GCMs. *Journal of the Atmospheric Sciences*, *71*, 3327–3349. https://doi.org/10.1175/JAS-D-13-0240.1

Bengtsson, L., Bao, J., Pegion, P., Penland, C., Michelson, S., & Whitaker, J. (2019). A model framework for stochastic representation of uncertainties associated with physical processes in NOAA's next generation global prediction system (NGGPS). *Monthly Weather Review*, *147*, 893–911.

Bengtsson, L., Dias, J., Gehne, M., Bechtold, P., Whitaker, J., Bao, J., et al. (2019). Convectively coupled equatorial wave simulations using the ECMWF IFS and the NOAA GFS cumulus convection schemes in the NOAA GFS model. *Monthly Weather Review*, *147*, 4005–4025. https://doi.org/10.1175/MWR-D-19-0195.1

Bengtsson, L., & Körnich, H. (2016). Impact of a stochastic parameterization of cumulus convection, using cellular automata, in a mesoscale ensemble prediction system. *Quarterly Journal of the Royal Meteorological Society*, *142*, 1150–1159. https://doi.org/10.1002/qj.2720

Bengtsson, L., Körnich, H., Källén, E., & Svensson, G. (2011). Large-scale dynamical response to subgrid scale organization provided by cellular automata. *Journal of the Atmospheric Sciences*, *68*, 3132–3144.

Bengtsson, L., Steinheimer, M., Bechtold, P., & Geleyn, J.-F. (2013). A stochastic parameterization for deep convection using cellular automata. *Quarterly Journal of the Royal Meteorological Society*, *139*, 1533–1543. https://doi.org/10.1002/qj.2108

Berner, J., Achatz, U., Batte, L., Bengtsson, L., De La Camara, A., Christensen, H. M., et al. (2017). Stochastic parameterization: Towards a new view of weather and climate models. *Bulletin of the American Meteorological Society*, *98*, 565–587. https://doi.org/10.1175/BAMS-D-15-00268.1

Böing, S. J. (2016). An object-based model for convective cold pool dynamics. *Mathematics of Climate and Weather Forecasting*, *2*(1), 43–60.

Buizza, R., Miller, M., & Palmer, T. (1999). Stochastic representation of model uncertainties in the ECMWF ensemble prediction system. *Quarterly Journal of the Royal Meteorological Society*, *125*, 2887–2908.

Chen, J.-H., & Lin, S.-J. (2013). Seasonal predictions of tropical cyclones using a 25-km-resolution general circulation model. *Journal of Climate*, *26*, 380–398. https://doi.org/10.1175/JCLI-D-12-00061.1

Chikira, M., & Sugiyama, M. (2010). A cumulus parameterization with state-dependent entrainment rate. Part I: Description and sensitivity to temperature and humidity profiles. *Journal of the Atmospheric Sciences*, *67*, 2171–2193. https://doi.org/10.1175/2010JAS3316.1
Chopard, B., & Droz, M. (1998). *Cellular automata modeling of physical systems*. Cambridge, UK: Cambridge University Press.
Christensen, H. M., Berner, J., Coleman, D. R., & Palmer, T. N. (2017). Stochastic parameterization and El Niño–southern oscillation. *Journal of Climate*, *30*, 17–38. https://doi.org/10.1175/JCLI-D-16-0122.1
Deans, S. R. (1983). *The Radon transform and some of its applications* (p. 295). New York, NY: John Wiley & Sons.
Dee, D. P., Uppala, S. M., Simmons, A. J., Berrisford, P., Poli, P., Kobayashi, S., et al. (2011). The ERA-Interim reanalysis: Configuration and performance of the data assimilation system. *Quarterly Journal of the Royal Meteorological Society*, *137*(656), 553–597. https://doi.org/10.1002/qj.828
Dias, J., Gehne, M., Kiladis, G. N., Sakaeda, N., Bechtold, P., & Haiden, T. (2018). Equatorial waves and the skill of NCEP and ECMWF numerical weather prediction systems. *Monthly Weather Review*, *146*, 1763–1784. https://doi.org/10.1175/MWR-D-17-0362.1
Dias, J., & Kiladis, G. N. (2014). Influence of the basic state zonal flow on convectively coupled equatorial waves. *Geophysical Research Letters*, *41*, 6904–6913. https://doi.org/10.1002/2014GL061476
Dias, J., & Pauluis, O. (2011). Modulations of the phase speed of convectively coupled Kelvin waves by the ITCZ. *Journal of the Atmospheric Sciences*, *68*, 1446–1459. https://doi.org/10.1175/2011JAS3630.1
Donner, L. J. (1993). A cumulus parameterization including mass fluxes, vertical momentum dynamics, and mesoscale effects. *Journal of the Atmospheric Sciences*, *50*, 889–906. https://doi.org/10.1175/1520-0469(1993)050<0889:ACPIMF>2.0.CO;2
Donner, L. J., Seaman, C. J., Hemler, R. S., & Fan, S. (2001). A cumulus parameterization scheme including mass fluxes, convective vertical velocities, and mesoscale effects: Thermodynamic and hydrological aspects in a general circulation model. *Journal of Climate*, *14*, 3444–3463.
Dorrestijn, J., Crommelin, D., Biello, J., & Böing, S. (2013). A data-driven multicloud model for stochastic parametrization of deep convection. *Philosophical Transactions of the Royal Society*, *371*(20120374). https://doi.org/10.1098/rsta.2012.0374
Dorrestijn, J., Crommelin, D. T., Siebesma, A. P., Jonker, H. J., & Jakob, C. (2015). Stochastic parameterization of convective area fractions with a multicloud model inferred from observational data. *Journal of the Atmospheric Sciences*, *72*, 854–869.
Frierson, D. M. W. (2007). Convectively coupled Kelvin waves in an idealized moist general circulation model. *Journal of the Atmospheric Sciences*, *64*, 2076–2090. https://doi.org/10.1175/JAS3945.1
Frierson, D. M. W., Kim, D., Kang, I.-S., Lee, M.-I., & Lin, J. (2011). Structure of AGCM-simulated convectively coupled Kelvin waves and sensitivity to convective parameterization. *Journal of the Atmospheric Sciences*, *68*, 26–45. https://doi.org/10.1175/2010JAS3356.1
Fuchs, Ž. (2015). Tropical dynamics: Large-scale convectively coupled waves. In R. S. Plant, & J.-I. Yano (Eds.), *Chapter 5 in book parameterization of atmospheric convection* (pp. 147–169). London, UK: World Scientific.
Fuchs, Ž., Gjorgjievska, S., & Raymond, D. J. (2012). Effects of varying the shape of the convective heating profile on convectively coupled gravity waves and moisture modes. *Journal of the Atmospheric Sciences*, *69*, 2505–2519. https://doi.org/10.1175/JAS-D-11-0308.1
Fuchs, Ž., & Raymond, D. J. (2007). A simple, vertically resolved model of tropical disturbances with a humidity closure. *Tellus A*, *59*, 344–354. https://doi.org/10.1111/j.1600-0870.2007.00230.x
Gerard, L., Piriou, J. M., Brožková, R., Geleyn, J. F., & Banciu, D. (2009). Cloud and precipitation parametrization in a meso-gamma scale operational weather prediction model. *Monthly Weather Review*, *137*, 3960–3977.
Gottwald, G. A., Peters, K., & Davies, L. (2016). A data-driven method for the stochastic parameterization of subgrid-scale tropical convective area fraction. *Quarterly Journal of the Royal Meteorological Society*, *142*, 349–359. https://doi.org/10.1002/qj.2655
Hagos, S., Feng, Z., Plant, R. S., Houze, R. A., & Xiao, H. (2018). A stochastic framework for modeling the population dynamics of convective clouds. *Journal of Advances in Modeling Earth Systems*, *10*, 448–465. https://doi.org/10.1002/2017MS001214
Han, Y., & Khouider, B. (2010). Convectively coupled waves in a sheared environment. *Journal of the Atmospheric Sciences*, *67*(9), 2913–2942. https://doi.org/10.1175/2010JAS3335.1
Hannah, W. M., & Maloney, E. D. (2011). The role of moisture-convection feedbacks in simulating the Madden-Julian oscillation. *Journal of Climate*, *24*, 2754–2770. https://doi.org/10.1175/2011JCLI3803.1
Hannah, W. M., & Maloney, E. D. (2014). The moist static energy budget in NCAR CAM5 hindcasts during DYNAMO. *Journal of Advances in Modeling Earth Systems*, *6*(2), 420–440. https://doi.org/10.1002/2013ms000272
Han, J., & Pan, H. (2011). Revision of convection and vertical diffusion schemes in the NCEP Global Forecast System. *Weather and Forecasting*, *26*, 520–533. https://doi.org/10.1175/WAF-D-10-05038.1
Han, J., Wang, W., Kwon, Y. C., Hong, S., Tallapragada, V., & Yang, F. (2017). Updates in the NCEP GFS cumulus convection schemes with scale and aerosol awareness. *Weather and Forecasting*, *32*, 2005–2017. https://doi.org/10.1175/WAF-D-17-0046.1
Han, J., Witek, M. L., Teixeira, J., Sun, R., Pan, H., Fletcher, J. K., & Bretherton, C. S. (2016). Implementation in the NCEP GFS of a hybrid eddy-diffusivity mass-flux (EDMF) boundary layer parameterization with dissipative heating and modified stable boundary layer mixing. *Weather and Forecasting*, *31*, 341–352. https://doi.org/10.1175/WAF-D-15-0053.1
Harris, L. M., Lin, S., & Tu, C. (2016). High-resolution climate simulations using GFDL HiRAM with a stretched global grid. *Journal of Climate*, *29*, 4293–4314. https://doi.org/10.1175/JCLI-D-15-0389.1
Hong, S.-Y., & Pan, H.-L. (1996). Nonlocal boundary layer vertical diffusion in a medium-range forecast model. *Monthly Weather Review*, *124*, 2322–2339. https://doi.org/10.1175/1520-0493(1996)124<2322:NBLVDI>2.0.CO;2
Houze, R. A., Jr. (2004). Mesoscale convective systems. *Reviews of Geophysics*, *42*, RG4003. https://doi.org/10.1029/2004RG000150
Hovmöller, E. (1949). The trough-and-ridge diagram. *Tellus*, *1*, 62–66. https://doi.org/10.1111/j.2153-3490.1949.tb01260.x
Huang, X.-Y. (1988). The organization of moist convection by internal gravity waves. *Tellus*, *42A*, 270–285.
Huffman, G. J., Bolvin, D., Nelkin, E., Wolff, D., Adler, R., Gu, G., et al. (2007). The TRMM Multisatellite Precipitation Analysis (TMPA): Quasi-global, multiyear, combined-sensor precipitation estimates at fine scales. *Journal of Hydrometeorology*, *8*, 38–55. https://doi.org/10.1175/JHM560.1
Inoue, K., & Back, L. (2015a). Column-integrated moist static energy budget analysis on various time scales during TOGA COARE. *Journal of the Atmospheric Sciences*, *72*, 1856–1871. https://doi.org/10.1175/JAS-D-14-0249.1
Inoue, K., & Back, L. E. (2015b). Gross moist stability assessment during TOGA COARE: Various interpretations of gross moist stability. *Journal of the Atmospheric Sciences*, *72*, 4148–4166. https://doi.org/10.1175/JAS-D-15-0092.1
Jones, C., Gottschalck, J., Carvalho, L. M. V., & Higgins, W. (2011). Influence of the Madden–Julian oscillation on forecasts of extreme precipitation in the contiguous United States. *Monthly Weather Review*, *139*, 332–350. https://doi.org/10.1175/2010MWR3512.1
Joyce, R. J., Janowiak, J. E., Arkin, P. A., & Xie, P. (2004). CMORPH: A method that produces global precipitation estimates from passive microwave and infrared data at high spatial and temporal resolution. *Journal of Hydrometeorology*, *5*, 487–503. https://doi.org/10.1175/1525-7541(2004)005,0487:CAMTPG.2.0.CO;2

Jung, T., Palmer, T. N., Rodwell, M. J., & Serrar, S. (2010). Understanding the anomalously cold European winter of 2005/06 using relaxation experiments. *Monthly Weather Review*, *138*(8), 3157–3174. https://doi.org/10.1175/2010MWR3258.1

Jung, T., Vitart, F., Ferranti, L., & Morcrette, J. J. (2011). Origin and predictability of the extreme negative NAO winter of 2009/10. *Geophysical Research Letters*, *38*, L07701. https://doi.org/10.1029/2011GL046786

Kessler, W. S., & Kleeman, R. (2000). Rectification of the Madden-Julian oscillation into the ENSO cycle. *Journal of Climate*, *13*, 3560–3575.

Khouider, B., Biello, J., & Majda, A. (2010). A stochastic multicloud model for tropical convection. *Communications in Mathematical Sciences*, *8*, 187–216.

Kiladis, G., Wheeler, M., Haertel, P., Straub, K., & Roundy, P. E. (2009). Convectively coupled equatorial waves. *Reviews of Geophysics*, *47*, RG2003. https://doi.org/10.1029/2008RG000266

Kim, J., & Alexander, M. J. (2013). Tropical precipitation variability and convectively coupled equatorial waves on submonthly time scales in reanalyzes and TRMM. *Journal of Climate*, *26*, 3013–3030. https://doi.org/10.1175/JCLI-D-12-00353.1

Leutbecher, M., Lock, S.-J., Ollinaho, P., Lang, S., Balsamo, G., Bechtold, P., et al. (2017). Stochastic representations of model uncertainties at ECMWF: State of the art and future vision. *Quarterly Journal of the Royal Meteorological Society*, *143*, 2315–2339. https://doi.org/10.1002/qj.3094

Lin, S. (2004). A "vertically Lagrangian" finite-volume dynamical core for global models. *Monthly Weather Review*, *132*, 2293–2307. https://doi.org/10.1175/1520-0493(2004)132<2293:AVLFDC>2.0.CO;2

Lin, Y.-L., Farley, R. D., & Orville, H. D. (1983). Bulk parameterization of the snow field in a cloud model. *Journal of Climate and Applied Meteorology*, *22*, 1065–1092. https://doi.org/10.1175/1520-0450(1983)022<1065:BPOTSF>2.0.CO;2

Lin, S., & Rood, R. B. (1996). Multidimensional flux-form semi-Lagrangian transport schemes. *Monthly Weather Review*, *124*, 2046–2070. https://doi.org/10.1175/1520-0493(1996)124<2046:MFFSLT>2.0.CO;2

Mapes, B., & Neale, R. (2011). Parameterizing convective organization to escape the entrainment dilemma. *Journal of Advances in Modeling Earth Systems*, *3*(2). https://doi.org/10.1029/2011ms000042

Moncrieff, M. W., Liu, C., & Bogenschutz, P. (2017). Simulation, modeling, and dynamically based parameterization of organized tropical convection for global climate models. *Journal of the Atmospheric Sciences*, *74*, 1363–1380. https://doi.org/10.1175/JAS-D-16-0166.1

Moncrieff, M. W., Waliser, D. E., Miller, M. J., Shapiro, M. A., Asrar, G. R., & Caughey, J. (2012). Multiscale convective organization and the YOTC virtual global field campaign. *Bulletin of the American Meteorological Society*, *93*, 1171–1187. https://doi.org/10.1175/BAMS-D-11-00233.1

Morton, B. R., Taylor, G., & Turner, J. (1956). Turbulent gravitational convection from maintained and instantaneous sources. *Proceedings of the Royal Society of London. Series A. Mathematical and Physical Sciences*, *234*(1196), 1–23. https://doi.org/10.1098/rspa.1956.0011

Neelin, J. D., & Held, I. M. (1987). Modeling tropical convergence based on the moist static energy budget. *Monthly Weather Review*, *115*, 3–12. https://doi.org/10.1175/1520-0493(1987)1152.0.CO;2

Neggers, R. A. J. (2015). Exploring bin-macrophysics models for moist convective transport and clouds. *Journal of Advances in Modeling Earth Systems*, *7*, 2079–2104. https://doi.org/10.1002/2015MS000502

Palmer, T. N., Buizza, R., Doblas-Reyes, F., Jung, T., Leutbecher, M., Shutts, G., et al. (2009). Stochastic parametrization and model uncertainty. *ECMWF Technical Memorandum.*, *598*, 44. Retrieved from https://www.ecmwf.int/sites/default/files/elibrary/2009/11577-stochastic-parametrization-and-model-uncertainty.pdf

Pan, H.-L., & Wu, W.-S. (1995). Implementing a mass flux convective parameterization package for the NMC Medium-Range Forecast model. *NMC Office Note*, *409*, 40. https://repository.library.noaa.gov/view/noaa/11429

Park, S. (2014). A unified convection scheme (UNICON). Part I: Formulation. *Journal of the Atmospheric Sciences*, *71*, 3902–3930.

Plant, R. S. (2012). A new modelling framework for statistical cumulus dynamics. *Philosophical Transactions of the Royal Society A*, *370A*, 1041–1060. https://doi.org/10.1098/rsta.2011.0377

Raymond, D. J., & Fuchs, Ž. (2009). Moisture modes and the Madden-Julian oscillation. *Journal of Climate*, *22*, 3031–3046. https://doi.org/10.1175/2008JCLI2739.1

Raymond, D. J., Sessions, S. L., & Fuchs, Ž. (2007). A theory for the spinup of tropical depressions. *Quarterly Journal of the Royal Meteorological Society*, *133*, 1743–1754. https://doi.org/10.1002/qj.125

Raymond, D. J., Sessions, S. L., Sobel, A. H., & Fuchs, Ž. (2009). The mechanics of gross moist stability. *Journal of Advances in Modeling Earth Systems*, *1*, 9. https://doi.org/10.3894/JAMES.2009.1.9

Ricciardulli, L., & Sardeshmukh, P. D. (2002). Local time- and space scales of organized tropical deep convection. *Journal of Climate*, *15*, 2775–2790. https://doi.org/10.1175/1520-0442(2002)015<2775:LTASSO>2.0.CO;2

Schiro, K. A., & Neelin, J. D. (2019). Deep convective organization, moisture vertical structure, and convective transition using deep-inflow mixing. *Journal of the Atmospheric Sciences*, *76*, 965–987. https://doi.org/10.1175/JAS-D-18-0122.1

Schreck, C. J., Cordeira, J. M., & Margolin, D. (2013). Which MJO events affect North American temperatures? *Monthly Weather Review*, *141*, 3840–3850. https://doi.org/10.1175/MWR-D-13-00118.1

Siebesma, A. P., Soares, P. M. M., & Teixeira, J. (2007). A combined eddy-diffusivity mass-flux approach for the convective boundary layer. *Journal of the Atmospheric Sciences*, *64*, 1230–1248. https://doi.org/10.1175/JAS3888.1

Sobel, A. H., & Bretherton, C. S. (2003). Large-scale waves interacting with deep convection in idealized mesoscale model simulations. *Tellus A*, *55*, 45–60. https://doi.org/10.1034/j.1600-0870.2003.201421.x

Sobel, A., & Maloney, E. (2012). An idealized semi-empirical framework for modeling the Madden-Julian oscillation. *Journal of the Atmospheric Sciences*, *69*, 1691–1705. https://doi.org/10.1175/JAS-D-11-0118.1

Sobel, A., & Maloney, E. (2013). Moisture modes and the eastward propagation of the MJO. *Journal of the Atmospheric Sciences*, *70*, 187–192. https://doi.org/10.1175/JAS-D-12-0189.1

Sugiyama, M. (2009). The moisture mode in the quasi-equilibrium tropical circulation model. part I: Analysis based on the weak temperature gradient approximation. *Journal of the Atmospheric Sciences*, *66*, 1507–1523. https://doi.org/10.1175/2008JAS2690.1

Tompkins, A. M. (2001). Organization of tropical convection in low vertical wind shears: The role of water vapor. *Journal of the Atmospheric Sciences*, *58*, 529–545.

Troen, I., & Mahrt, L. (1986). A simple model of the atmospheric boundary layer sensitivity to surface evaporation. *Boundary Layer Meteorology*, *37*, 129–148. https://doi.org/10.1007/BF00122760

Tulich, S. N., & Kiladis, G. N. (2012). Squall lines and convectively coupled gravity waves in the tropics: Why do most cloud systems propagate westward? *Journal of the Atmospheric Sciences*, *69*, 2995–3012. https://doi.org/10.1175/JAS-D-11-0297.1

Turner, J. S., & Yang, I. K. (1963). Turbulent mixing at the top of stratocumulus clouds. *Journal of Fluid Mechanics*, *17*, 212–224.

Vitart, F., & Molteni, F. (2010). Simulation of the Madden–Julian oscillation and its teleconnections in the ECMWF forecast system. *Quarterly Journal of the Royal Meteorological Society*, *136*, 842–855.

Wang, B., & Chen, J. (1989). On the zonal-scale selection and vertical structure of equatorial intraseasonal waves. *Quarterly Journal of the Royal Meteorological Society*, *115*(490), 1301–1323. https://doi.org/10.1002/qj.49711549007

Wheeler, M., & Kiladis, G. (1999). Convectively coupled equatorial waves: Analysis of clouds and temperature in the wavenumber–frequency domain. *Journal of the Atmospheric Sciences*, *56*, 374–399.

Yang, C., Christensen, H. M., Corti, S., von Hardenberg, J., & Davini, P. (2019). The impact of stochastic physics on the El Niño Southern Oscillation in the EC-Earth coupled model. *Climate Dynamics*, *53*, 2843–2859. https://doi.org/10.1007/s00382-019-04660-0

Yang, G.-Y., Hoskins, B., & Slingo, J. (2007). Convectively coupled equatorial waves. Part II: Propagation characteristics. *Journal of the Atmospheric Sciences*, *64*, 3424–3437.

Zhang, C. (2005). Madden-Julian oscillation. *Reviews of Geophysics*, *43*, RG2003. https://doi.org/10.1029/2004RG000158

Zhang, C., & Webster, P. J. (1989). Effects of zonal flows on equatorially trapped waves. *Journal of the Atmospheric Sciences*, *46*(24), 3632–3652. https://doi.org/10.1175/1520-0469(1989)046/3632:EOZFOE/2.0.CO;2